

Study of Straight-Line-Type Sagnac Optical Fiber Acoustic Sensing System

Jiang Wang ¹, Ruixi Tang ², Jianjun Chen ^{2,*} , Ning Wang ³, Yong Zhu ³, Jie Zhang ³ and Juan Ruan ²

¹ The Institute of Xi'an Aerospace Solid Propulsion Technology, Xi'an 710025, China

² The Key Laboratory of Electromagnetic Technology and Engineering, China West Normal University, Nanchong 637000, China

³ The Key Laboratory of Optoelectronic Technology & System, Education Ministry of China, Chongqing University, Chongqing 400044, China

* Correspondence: jianjchen@cwnu.edu.cn; Tel.: +86-13509406989

Abstract: A straight-line-type Sagnac optic fiber acoustic sensing system is proposed in this paper to adopt the application needs of no man's plateau borderline for monitoring mechanical invasion. The Sagnac interference fiber loop is replaced by a straight-line fiber and a 1×2 coupler, and the length of the Sagnac interference fiber loop is shortened by close to 50%. The influences of delay fiber and sensing fiber on the sensing system are analyzed by theory calculation and simulation and the optimal lengths of delay fiber and sensing fiber were decided. The experiment system was set, and the sensing fiber was wound into titanium alloy cylinder to compose the sensing element. Experimental results show that the sensing system has a good response to 50–8000 Hz and 70 dB sinusoidal acoustical signals and can well distinguish the signals of different frequencies. Using a small-scale helicopter audio signal as the acoustical signal, the test results show that the response curve is consistent with the simulation results and the sensitivity reaches 30.67 mV/Pa.

Keywords: acoustic detection; optical fiber sensing; Sagnac interference; straight-line type



Citation: Wang, J.; Tang, R.; Chen, J.; Wang, N.; Zhu, Y.; Zhang, J.; Ruan, J. Study of Straight-Line-Type Sagnac Optical Fiber Acoustic Sensing System. *Photonics* **2023**, *10*, 83.

<https://doi.org/10.3390/photonics10010083>

Received: 8 December 2022

Revised: 7 January 2023

Accepted: 9 January 2023

Published: 11 January 2023



Copyright: © 2023 by the authors. Licensee MDPI, Basel, Switzerland. This article is an open access article distributed under the terms and conditions of the Creative Commons Attribution (CC BY) license (<https://creativecommons.org/licenses/by/4.0/>).

1. Introduction

Optical fiber acoustic sensing technology has broad application prospects in perimeter security, environmental noise monitoring, nondestructive monitoring, etc. [1]. Compared with traditional electroacoustic sensors, photoacoustic sensors have the advantages of high temperature and humidity resistance, anti-electromagnetic interference, and corrosion resistance, which make them the hot spot of acoustic sensing technology research [2–6]. Presently, interferometric fiber optic acoustic sensors are mainly based on the principles of Michelson interference, fiber optic Fabry–Perot interference, Mach–Zehnder interference, and Sagnac interference [7–13]. The photoacoustic sensing system based on the Michelson interferometer and Fabry–Perot interferometer requires high-precision machining technology and accurate alignment of components, which leads to poor environmental adaptability and is limited to applications in harsh natural environments [14]. Mach–Zehnder interferometric photoacoustic sensors have the disadvantages of low sensitivity and low signal-to-noise ratio (SNR) [15–17]. The photoacoustic sensing system based on Sagnac interference has high sensitivity, wide bandwidth, and high signal-to-noise ratio and only uses optic fiber as the sensitive elements without any fiber structure changes, which makes it become a cheap and reliable choice for sound detection in harsh environments, especially when it applied in no man's plateau borderline for monitoring the invasion of military motor vehicles, armored cars, unmanned aerial vehicles, etc. [18–20].

When a photoacoustic sensing system based on a Sagnac interferometer is operated in a natural environment, a large amount of non-sensing fiber of the Sagnac loop is exposed to environmental vibration and noise [18]. The acoustic detection sensitivity, SNR, and stability will be significantly reduced by disturbances in the non-sensing optical fiber.

The traditional solution is to add anti-vibration and anti-wear protection for non-acoustic sensing fiber [18]. However, this method greatly increases the application cost, especially when the length of the signal transmission fiber is long. Meanwhile, the signal transmission fiber with protection cannot completely eliminate the problems of sensitivity and stability reduction. Therefore, shortening the length of signal transmission fiber becomes a good idea for solving this problem.

2. Sensor Configuration and Theory Analysis

As shown in Figure 1, the traditional Sagnac fiber optic acoustic sensor has a long Sagnac interference optic fiber loop. When the long optic fiber loop is exposed to the natural environment, severe noise appears at the detector. As shown in Figure 2, a schematic diagram of the straight-line-type Sagnac fiber optic acoustic sensing system was proposed. Compared to the traditional Sagnac fiber optic acoustic sensor, the two light beams of the CW (clockwise) and CCW (counterclockwise) pass coupler C_2 are transmitted by one fiber. At coupler 3, the beams pass it and come back to the optic fiber again. Because of the improvement in the Sagnac loop, one arm of the loop disappeared, which means the transmission fiber is reduced by nearly 50%. The straight-line-type Sagnac fiber optic acoustic sensing system shortens the lengths of the Sagnac loop and reduces the disturbance of environments.

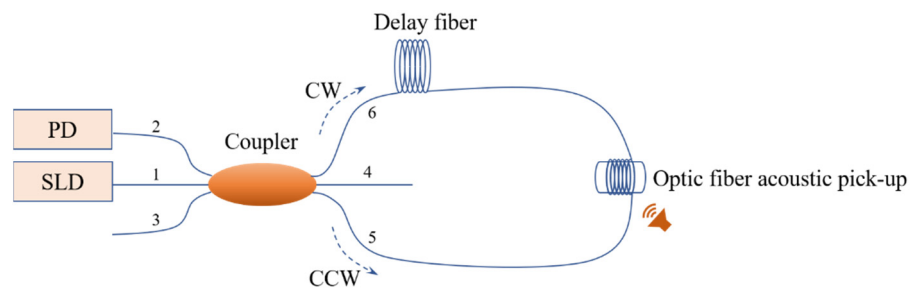


Figure 1. A schematic diagram of traditional Sagnac fiber optic acoustic sensor.

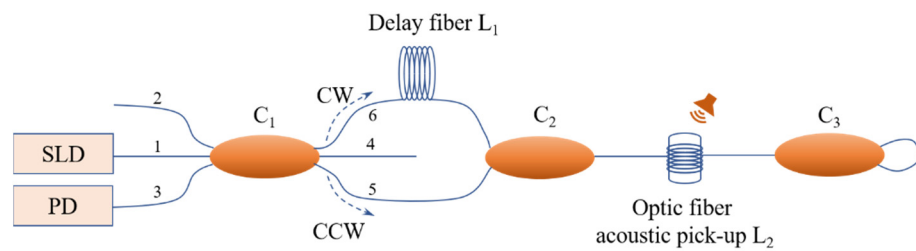


Figure 2. A schematic diagram of straight-line-type Sagnac fiber optic acoustic sensor.

The light emitted by a super-luminescent light-emitting diode (SLD) passes 3×3 coupler C_1 and can be divided into three beams, and then two beams enter the CW (clockwise) and CCW (counterclockwise) optical paths through port 6 and 5. At coupler C_2 , the two beams are merged into one single beam and transmitted to optic fiber acoustic pick-up L_2 . At coupler C_3 , the light is divided into two beams and comes back through port 2 and 3 of C_3 . When the two beams come back to C_1 , interference occurs and is detected by the photoelectric detector (PD). During this process, there are four main optical paths, as follows.

- A: 1—6— L_1 — C_2 — L_2 — C_3 — L_2 — C_2 — L_1 —6— C_1 ;
- B: 1—6— L_1 — C_2 — L_2 — C_3 — L_2 — C_2 —5— C_1 ;
- C: 1—5— C_2 — L_2 — C_3 — L_2 — C_2 — L_1 —6— C_1 ;
- D: 1—5— C_2 — L_2 — C_3 — L_2 — C_2 —5— C_1 .

In the four optical paths, path A is the longest, path D is the shortest, and paths B and C are equal. When a broadband light source is used, the coherence length is very short and only optical paths B and C can find a recognizable interference in coupler C_1 .

The interference light intensity in C_1 can be expressed as

$$I = \frac{1}{9}I_0[1 + \cos(\Delta\varphi + \Delta\psi)] \tag{1}$$

where I is the interference light intensity, I_0 is the light intensity of SLD coupled into the optical fiber, $\Delta\varphi$ is the phase difference caused by sound pressure, and $\Delta\psi$ is the phase shift caused by coupler C_1 . The sensing light beam passes the optic fiber acoustic pick-up L_2 twice, so the practical acoustic sensing fiber length is two-times the optic fiber acoustic pick-up L_2 , and the sensitivity is obviously higher than the traditional Sagnac fiber optic acoustic sensing system. The phase sensitivity of the straight-line-type Sagnac fiber optic acoustic sensing system under 1Pa sound pressure can be expressed as

$$S = \frac{8\pi nkL_2}{\lambda} \sin \frac{n\pi L_1 f}{c} \tag{2}$$

where S is the phase sensitivity, L_2 is the length of the optic fiber acoustic pick-up, L_1 is the length of the delay fiber, n is the refractive index of silica fiber, k is the elastic coefficient of optical fiber, f is the sound frequency, λ is the optical wavelength, and c is the vacuum speed of light. The phase sensitivity expression shows that the phase sensitivity is linear to sensing fiber loop L_2 and is sinusoidal to delay fiber loop L_1 . For a definite sound pressure P , the phase difference caused by the sound pressure can be calculated by

$$\Delta\varphi = SP = \left[\frac{8\pi nkL_2}{\lambda} \sin \left(\frac{n\pi L_1 f}{c} \right) \right] P \tag{3}$$

Substituting Equation (3) into Equation (1), the interference light intensity received by PD is shown as

$$I = \frac{1}{9}I_0 \left\{ 1 + \cos \left[\frac{8\pi nkL_2}{\lambda} P \sin \left(\frac{n\pi L_1 f}{c} \right) + \Delta\psi \right] \right\} \tag{4}$$

When a 3×3 coupler is used, the phase shift caused by the coupler is $\Delta\psi = 2\pi/3$. For a certain sensing system and a certain invader, the initial light intensity, light wavelength, elastic coefficient, sound pressure, and the frequency of sound are all certain. Then, the interference light intensity received by PD will mainly be influenced by the lengths of the sensing fiber and delay fiber.

When the system is used to monitor invasion of military motor vehicles, armored cars, unmanned aerial vehicles, etc., at the borderline, the sound-detection frequency is focused on 50–8000 Hz and the detection sound pressure level (SPL) range is often 50–100 dB. To confirm the best element parameters, a series of simulations is finished. In the simulations, $I_0 = 1.3 \text{ mW}$, $\lambda = 1310 \text{ nm}$, $n = 1.456$, $k = 6.829 \times 10^{-9} \text{ Pa}^{-1}$, $c = 3 \times 10^8 \text{ m/s}$.

When $f = 5000 \text{ Hz}$ and $L_2 = 20 \text{ m}$, the SPL is between 50 and 100 dB, and the length of the delay fiber is set to 1 km, 2 km, and 4 km. Under the influence of the delay fiber loop, the simulation curves of sound pressure and interference light intensity are shown in Figure 3. The results show that the longer the delay fiber loop, the shorter period of interference light intensity and higher sensitivity of photoacoustic detection. However, as the length of the delay fiber loop increases, the linear detection range of sound pressure becomes narrower. When the delay fiber loop length is 4 km, although the sensitivity is higher, there is a crest at 98 dB and the linearity of the response curve becomes poor. When the delay fiber loop is 1 km, the sensitivity is lower. When the delay fiber loop is 2 km, the sensitivity is high and there is no peak and trough during 50–100 dB. Considering the balance of sensitivity and detection range, a 2 km delay optic fiber length is the best choice.

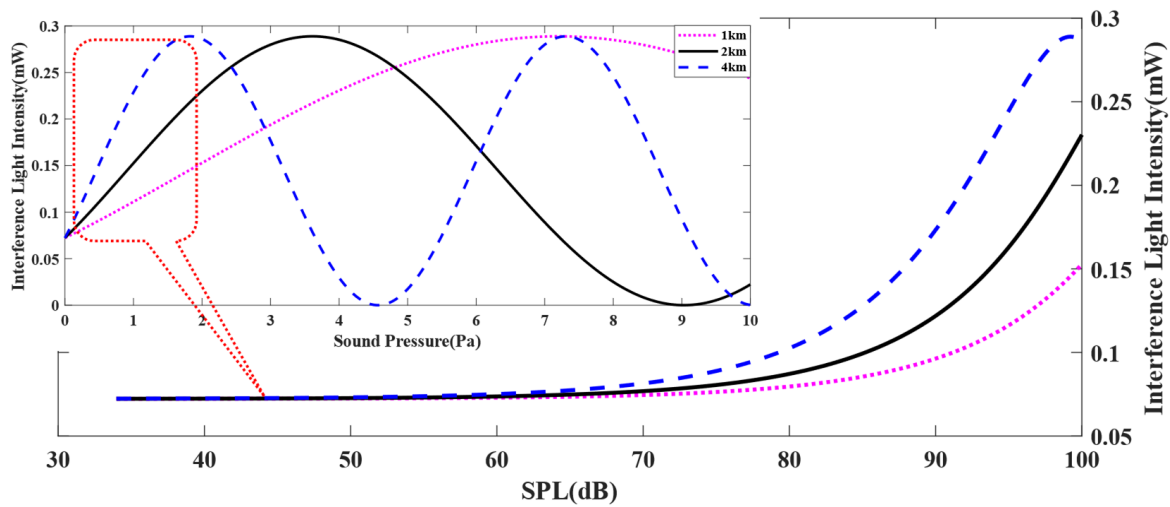


Figure 3. The influence of delay fiber length.

When $f = 5000$ Hz and $L_1 = 2$ km, the SPL is between 50 and 100 dB, and the length of the sensing fiber is set to 10 m, 20 m, and 40 m, the influence of optic fiber acoustic pick-up to sound pressure and interference light intensity is shown in Figure 4. Similar to the effect of delay fiber, the longer the optic fiber acoustic pick-up is, the shorter period of interference light intensity and the higher sensitivity of photoacoustic detection are. As the length of optic fiber acoustic pick-up increases, the sound-pressure-detection range becomes narrower. When the sensing fiber length is 30 m, although the sensitivity is higher, the curve is close to the crest at 100 dB and the linearity of the response curve becomes poor. When the sensing fiber is 10 m, the sensitivity is lower. Considering the balance of sensitivity and detection range, 20 m sensing optic fiber is the best choice.

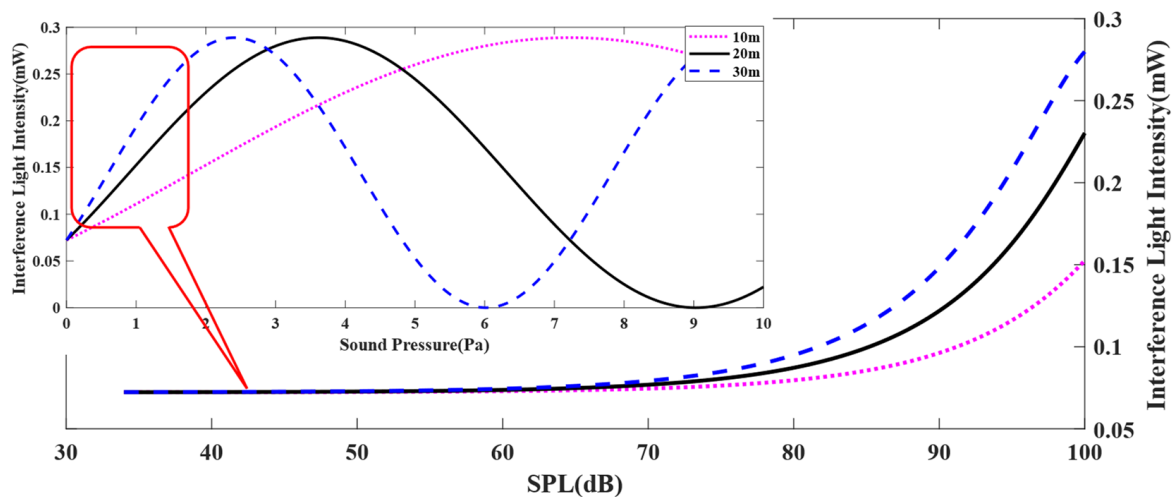


Figure 4. The influence of optic fiber acoustic pick-up length.

With the delay fiber is 2 km and optic fiber acoustic pick-up is 20 m, the influence of sound frequency and SPL on the interference light intensity is shown in Figure 5. When the sound frequency is 5000 Hz and the SPL is 50–100 dB, the relationship between interference light intensity and sound pressure will remain near linearity and there is no interference crest point in the sound-pressure range, which means there is no blind hearing problem. These results show that the designed system can be used as a sensor for sound detection with frequency 5000 Hz and SPL 50–100 dB.

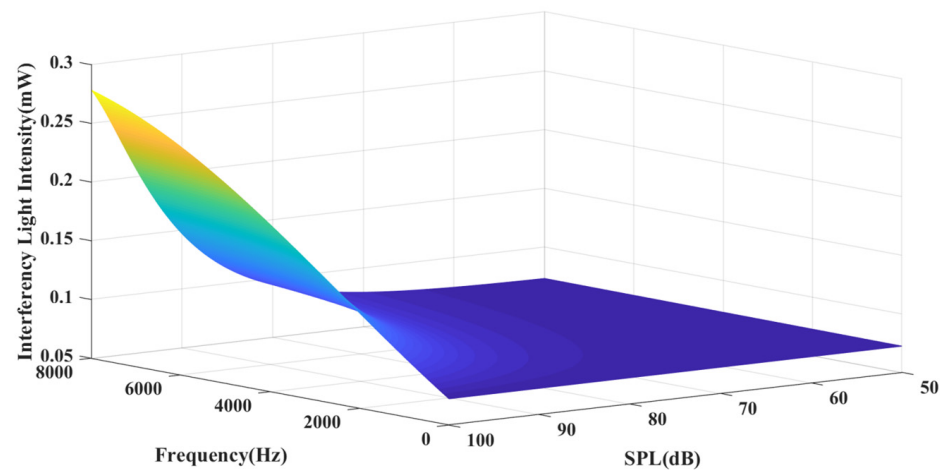


Figure 5. The simulation result of the straight-line-type Sagnac fiber optic acoustic sensor.

3. Experiments and Discussions

Figure 6 shows the experimental setup of the acoustic sensing system. An SLD (GR1346Q-A, made by the 44th Research Institute of CETC) was used as the light source. An InGaAs detector (GT322D, made by the 44th Research Institute of CETC) was used as the photoelectric detector (PD) in the testing system. The delay fiber used a single-mode silica fiber with a length of 2000 ± 5 m. The optic fiber acoustic pick-up was composed of titanium alloy cylinders and tightly wound single-mode silica optical fiber and the length of the sensing fiber was 20 ± 0.3 m. The interference signal acquisition and processing were finished by preprocessing circuit and LabView platform. The main parameters of SLD, PD, and DAQ (Data Acquisition) are shown in Table 1 and the spectrum of the source is shown in Figure 7.

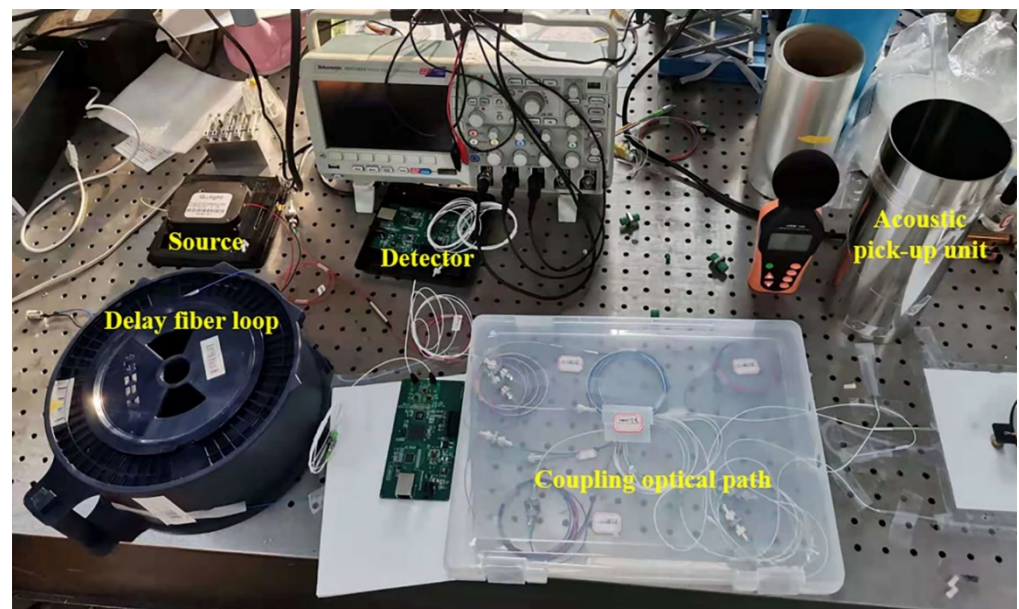


Figure 6. A photo of the testing system.

Table 1. The main parameters of the experiment setup.

SLD	PD	DAQ
Model: GR1346Q-A Central wavelength: 1296.5 nm Radiation power, ≥ 1 mW FWHM: Typ = 35 nm	model: GT322D Spectral Response Range: 900–1700 nm Responsivity: 0.7 A/w at 1310 nm −3 dB bandwidth: ≥ 1500 MHz	Type: UDP communication Sampling Frequency: 50 MHz Sampling Time: 16 ms

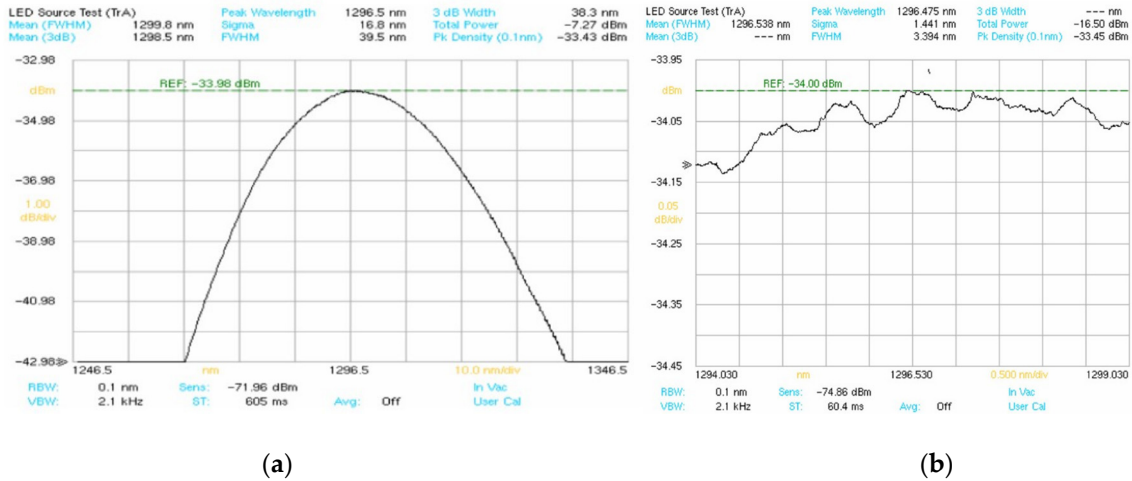


Figure 7. The tested spectrum of the source: (a) spectrum curve, (b) wavy curve around the central wavelength.

The response curves under different frequencies were tested. A 70 dB sinusoidal acoustical signal was used as an acoustic source, and the sampling frequency was set as 50 MHz. The audio signal frequencies firstly change between 500 and 8000 Hz, and the sampling time was 16 ms which ensures that signals of different frequencies are fully displayed. As shown in Figure 8, because the resonance frequency of the titanium alloy cylinder is about 4000 Hz, the optic acoustic sensing system has a good response to 500–8000 Hz acoustical signals, especially at 2000–6000 Hz, which covers the main frequency domain of the mechanical vehicles; the maximum output signal peak-to-peak response reaches 47.65 mV. The test results show that the frequency differences can be distinguished clearly from the curve, which means the different sounds are expected to be recognized from the output.

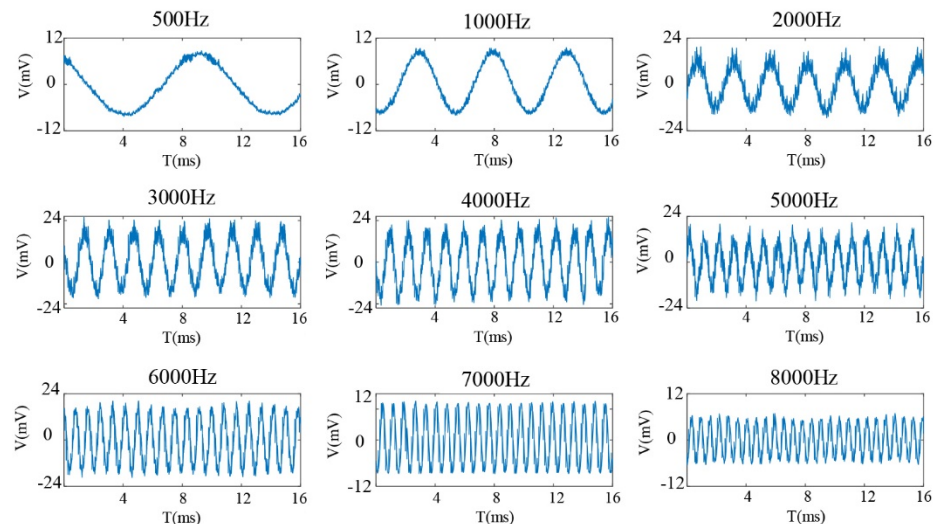


Figure 8. The responding curve of the sensing system to acoustical signals of 500–8000 Hz.

The lower limit of frequency response was tested. Figure 9 shows that the frequency difference between 50 Hz and 100 Hz can be distinguished, but the curve of 20 Hz becomes indiscernible.

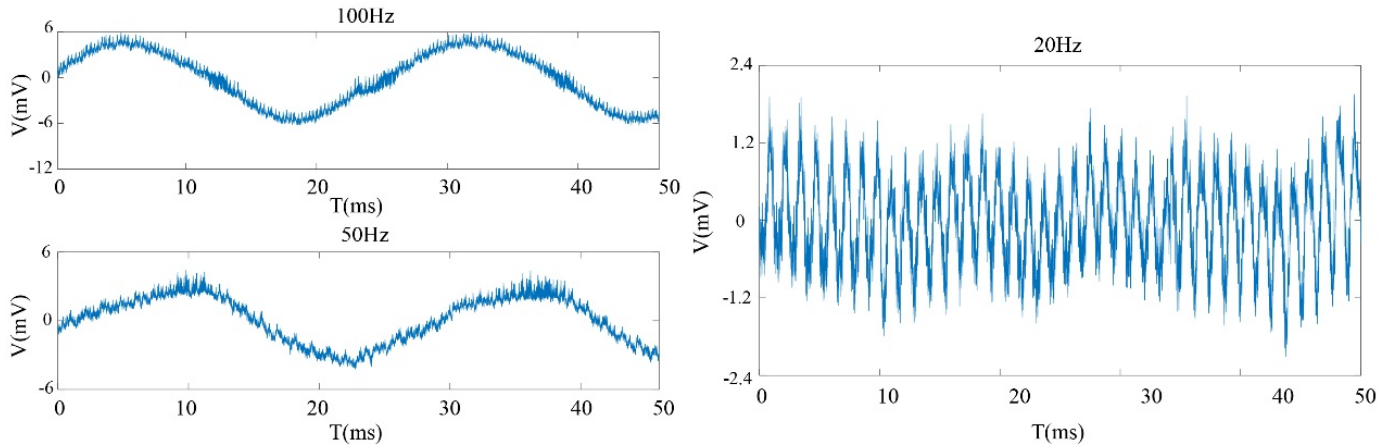


Figure 9. The responding curve of the sensor to acoustical signals of 100, 50, and 20 Hz.

All of the test results show that when the sound-pressure level is 70 dB, the peak-to-peak response of the sensing system to the pure sinusoidal acoustical signal of 50–8000 Hz is between 6.29 and 50.35 mV, and the interferential curve of the sound signal of different frequencies can be well distinguishable. The results also show that the response of the system under 50 Hz is very poor. The main reason is that the resonance frequency of the titanium alloy cylinder is about 4000 Hz, and when sound frequency is less than 50 Hz, the vibration of the titanium alloy cylinder becomes very weak. When the frequencies are more than 8000 Hz, the same problem will also appear on the system. However, in the application conditions of this paper, the frequencies of the military motor vehicles, armored cars, and unmanned aerial vehicles are often between 500 and 8000 Hz, so the system can meet application requirements well.

A test of the sensitivity of the sensing system was finished. An audio signal from a small-scale helicopter was used as the signal source and the SPL changed between 50 and 95 dB. The responding curve of the different SPL is tested and the statistical results of the test data are shown in Table 2. As shown in Figure 10, the test curve is matched with the simulation results, which are shown in Figures 3–5.

Table 2. Statistical table of the system response to sound data under different decibels.

SPL(dB)	50	55	60	65	70	75	80	85	90	95
Sound Pressure (Pa)	0.0063	0.011	0.02	0.036	0.063	0.11	0.2	0.36	0.63	2
Data Points Number	171	201	269	293	367	517	749	1266	2056	3543
Output Voltage (mV)	1.72	1.97	2.58	2.73	3.51	5.07	7.54	12.56	20.99	35.87

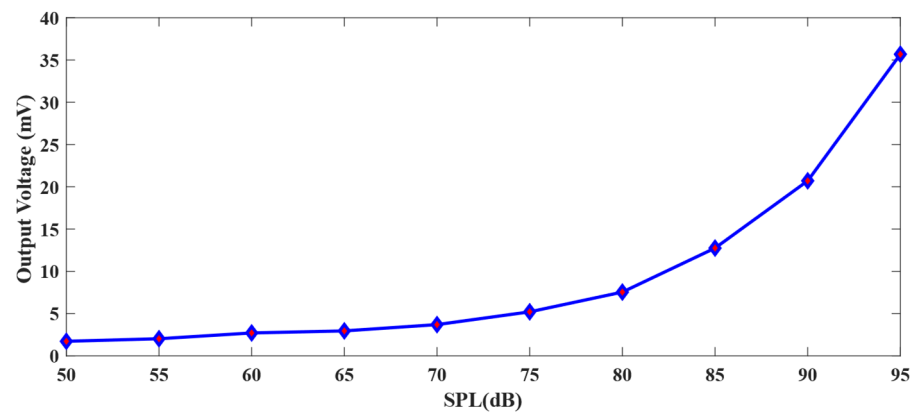


Figure 10. The response curve of SPL and output voltage.

As shown in Figure 11, the relationship between sound pressure and the output voltage was acquired, and the fitting curve was obtained using the least-square method. The equation of the fitting curve is

$$V = 30.67 \times P + 1.64 \tag{5}$$

where V is the output voltage of the sensing system and P is the sound pressure of the acoustical signal. The fitted equation shows that the equivalent output voltage varies linearly with the sound pressure, and the sensitivity of sound pressure detection is 30.67 mV/Pa in the linear responding region. The experimental results show that the system can accurately reflect the change in sound intensity, and the experimental results are in good agreement with the simulation results. The system has an application prospect in sound detection in harsh environments, such as no man’s borderline.

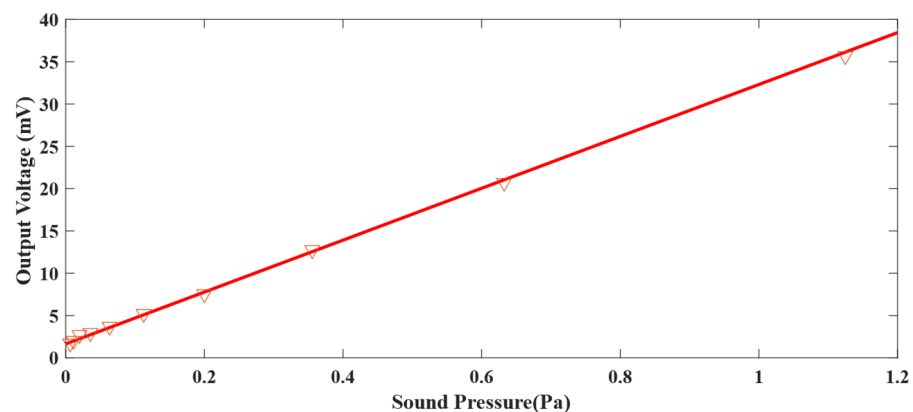


Figure 11. The test curve of sound pressure and output voltage.

4. Conclusions

In summary, a straight-line-type Sagnac fiber optic acoustic sensing system based on the Sagnac interference loop was proposed, which is utilized for sound detection and recognition of invading mechanical vehicles in harsh environments, such as the plateau borderline. The suitable lengths of delay fiber and sensing fiber were decided by theoretical calculation and simulation. In the experiment setup, the sensing fiber was tightly wound with titanium alloy cylinders to work as the acoustic sensing element. The test results show that the sensing system has a good response to the 50–8000 Hz acoustical signal at 70 dB and the acoustical signal can be distinguished by the interference curve. However, since the resonance frequency of the elastomer cylinder is around 4000 Hz, the system has a weak response to the acoustic signal, lower than 50 Hz and higher than 8000 Hz. When a small-scale helicopter audio signal is used as the signal source, the sensing system has a

good response in 50–100 dB, the output voltage varies linearly with sound pressure, and the sensitivity of sound pressure detection reaches 30.67 mV/Pa. The straight-line-type Sagnac fiber optic acoustic sensing system has obviously shortened the length of the Sagnac interference fiber loop and provides an available method for noise monitoring, perimeter security, and nondestructive monitoring. This work aimed to be applied on sound detection and identification in harsh work environments.

Author Contributions: Conceptualization, J.W. and J.C.; methodology, N.W. and J.C.; software, J.W. and R.T.; validation, J.W., J.C. and N.W.; formal analysis, J.C. and R.T.; investigation, J.R.; resources, Y.Z.; data curation, J.W. and R.T.; writing—original draft preparation, J.W. and R.T.; writing—review and editing, J.C. and J.Z.; visualization, J.W. and R.T.; supervision, Y.Z.; project administration, Y.Z.; funding acquisition, N.W. and J.C. All authors have read and agreed to the published version of the manuscript.

Funding: This research was funded by the National Natural Science Foundation of China, grant number 51875067 and “Sichuan Science and Technology Program, grant number 2021yj0541”.

Institutional Review Board Statement: Not applicable.

Informed Consent Statement: Not applicable.

Data Availability Statement: Not applicable.

Conflicts of Interest: The authors declare no conflict of interest.

References

1. Gorshkov, B.G.; Yüksel, K.; Fotiadi, A.A.; Wuilpart, M.; Korobko, D.A.; Zhirnov, A.A.; Stepanov, K.V.; Turov, A.T.; Konstantinov, Y.A.; Lobach, I.A. Scientific Applications of Distributed Acoustic Sensing: State-of-the-Art Review and Perspective. *Sensors* **2022**, *22*, 1033. [[CrossRef](#)] [[PubMed](#)]
2. He, Z.; Liu, Q. Optical Fiber Distributed Acoustic Sensors: A Review. *J. Light. Technol.* **2021**, *39*, 3671–3686. [[CrossRef](#)]
3. Sun, Y.; Li, H.; Fan, C.; Yan, B.; Chen, J.; Yan, Z.; Sun, Q. Review of a Specialty Fiber for Distributed Acoustic Sensing Technology. *Photonics* **2022**, *9*, 277. [[CrossRef](#)]
4. Pan, C.; Liu, X.; Zhu, H.; Shan, X.; Sun, X. Distributed optical fiber vibration sensor based on Sagnac interference in conjunction with OTDR. *Optics Express* **2017**, *25*, 20056–20070. [[CrossRef](#)] [[PubMed](#)]
5. Tang, J.; Cai, L.; Li, C.; Yang, M.; Guo, H.; Gan, W. Distributed acoustic sensors with wide frequency response based on UWFBG array utilizing dual-pulse detection. *Opt. Fiber Technol.* **2021**, *61*, 102452. [[CrossRef](#)]
6. Chen, Z.; He, J.; Xu, X.; He, J.; Xu, B.; Du, B.; Liao, C.; Wang, Y. High-Temperature Sensor Array Based on Fiber Bragg Gratings Fabricated by Femtosecond Laser Point-by-Point Method. *Acta Opt. Sin.* **2021**, *41*, 1306002.
7. Lalam, N.; Westbrook, P.S.; Li, J.; Lu, P.; Buric, M.P. Phase-Sensitive Optical Time Domain Reflectometry with Rayleigh Enhanced Optical Fiber. *IEEE Access* **2021**, *9*, 114428–114434. [[CrossRef](#)]
8. Ma, F.; Wang, X.; Wang, Y.; Zhu, R.; Yuan, Z.; Wang, P.; Yu, J.; Song, N. An improved device and demodulation method for fiber-optic distributed acoustic sensor based on homodyne detection. *Opt. Fiber Technol.* **2022**, *71*, 102925. [[CrossRef](#)]
9. Wang, J.; Zhao, J.; Wang, J.; Wan, H.; Zhang, Z. A multi-frequency fiber optic acoustic sensor based on graphene-oxide Fabry-Perot microcavity. *Opt. Fiber Technol.* **2021**, *65*, 102607. [[CrossRef](#)]
10. Yu, F.; Li, Z.; Okabe, Y. Application of a remotely bonded fiber-optic Bragg grating sensor to acoustic emission testing for a carbon-carbon composite at a temperature of 1000 °C. *Measurement* **2022**, *203*, 111908. [[CrossRef](#)]
11. Moradi, H.; Parvin, P.; Ojaghloo, A.; Shahi, F. Ultrasensitive fiber optic Fabry Pérot acoustic sensor using phase detection. *Measurement* **2021**, *172*, 108953. [[CrossRef](#)]
12. Stepanova, L.N.; Kabanov, S.I.; Chernova, V.V. Locating Acoustic Emission Signals Due to Shock Impacts on a Carbon Fiber Sample Using Piezoelectric and Fiber Optic Sensors. *Russ. J. Nondestruct. Test* **2022**, *58*, 237–247. [[CrossRef](#)]
13. Kislov, K.V.; Gravirov, V.V. Distributed Acoustic Sensing: A New Tool or a New Paradigm. *Seism. Instr.* **2022**, *58*, 485–508. [[CrossRef](#)]
14. Titov, S.A.; Machikhin, A.S.; Pozhar, V.E.; Bulatov, M.F. Study of the Ultrasonic Field in an Acousto-Optic Crystal Using Acoustic Methods. *J. Commun. Technol. Electron.* **2022**, *67*, 1443–1449. [[CrossRef](#)]
15. Ma, J.; He, Y.; Bai, X.; Sun, L.P.; Chen, K.; Oh, K.; Guan, B.O. Flexible microbubble-based Fabry-Pérot cavity for sensitive ultrasound detection and wide-view photoacoustic imaging. *Photon. Res.* **2020**, *8*, 1558–1565. [[CrossRef](#)]
16. Gao, X.K.; Ning, T.G.; Zhang, C.B.; Xu, J.; Zheng, J.J.; Lin, H.; Li, J.; Pei, L.; You, H.D. A dual-parameter fiber sensor based on few-mode fiber and fiber Bragg grating for strain and temperature sensing. *Opt. Commun.* **2020**, *454*, 124441. [[CrossRef](#)]
17. Xia, P.; Tan, Y.G.; Li, T.L.; Zhou, Z.D.; Lv, W.Q. A high-temperature resistant photonic crystal fiber sensor with single-side sliding Fabry-Perot cavity for super-large strain measurement. *Sens. Actuator A-Phys.* **2021**, *318*, 112492. [[CrossRef](#)]

18. Sun, L.P.; Yuan, Z.; Huang, T.; Sun, Z.; Lin, W.; Huang, Y.; Xiao, P.; Yang, M.; Li, J.; Bai-Ou Guan, B.-O. Ultrasensitive sensing in air based on Sagnac interferometer working at group birefringence turning point. *Opt. Express* **2019**, *27*, 29501–29509. [[CrossRef](#)] [[PubMed](#)]
19. Marin, J.M.; Ashry, I.; Alkhazragi, O.; Trichili, A.; Ng, T.K.; Ooi, B.S. Simultaneous distributed acoustic sensing and communication over a two-mode fiber. *Opt. Lett.* **2022**, *47*, 6321–6324. [[CrossRef](#)] [[PubMed](#)]
20. Chen, J.; Wang, J.; Wang, N.; Ruan, J.; Zhang, J.; Zhu, Y. An Improved Acoustic Pick-Up for Straight Line-Type Sagnac Fiber Optic Acoustic Sensing System. *Sensors* **2022**, *22*, 8193. [[CrossRef](#)] [[PubMed](#)]

Disclaimer/Publisher’s Note: The statements, opinions and data contained in all publications are solely those of the individual author(s) and contributor(s) and not of MDPI and/or the editor(s). MDPI and/or the editor(s) disclaim responsibility for any injury to people or property resulting from any ideas, methods, instructions or products referred to in the content.